Effect of lithiation on the elastic moduli of carbon fibres

Carbon 185 (2021) 234–241

Contents lists available at ScienceDirect

Carbon

journal homepage: www.elsevier.com/locate/carbon

Research Paper

Effect of lithiation on the elastic moduli of carbon fibres

Shanghong Duan [a], Anand H.S. Iyer [b], David Carlstedt [a], Florian Rittweger [c], Andrew Sharits [d, e], Calvin Maddox [d, e], Karl-Ragmar Riemschneider [c], David Mollenhauer [d], Magnus Colliander [b], Fang Liu [a], Leif E. Asp [a, *]

[a] Chalmers University of Technology, Department of Industrial and Materials Science, Gothenburg, Sweden
[b] Chalmers University of Technology, Department of Physics, Gothenburg, Sweden
[c] Hamburg University of Applied Sciences, Department of Information and Electrical Engineering, Hamburg, Germany
[d] Air Force Research Laboratory, AFRL/RXCC, Wright Patterson Airforce Base, Dayton, OH, USA
[e] UES Inc., Dayton, OH, USA

ARTICLE INFO

Article history:
Received 11 June 2021
Received in revised form
30 August 2021
Accepted 16 September 2021
Available online 20 September 2021

Keywords:
Carbon fiber electrode
Lithium-ion battery
Structural battery
Elastic modulus
Volume expansion

ABSTRACT

Carbon fibre electrodes can enable a solid-state battery to carry mechanical load as normal construction materials. The multifunctionality is promising for most lightweight applications. Like all electrode materials, both volume and elastic moduli of the carbon fibre electrodes change during battery cycling. Such changes jeopardize the mechanical integrity of the battery. Due to the challenging corrosion problem of the lithiated component in air, the effect of lithiation on the carbon fibre's elastic moduli has yet to be explored. Also, robust data on the expansion of carbon fibres from lithiation are lacking. In the present work, we demonstrate a method and perform tests of corrosion protected carbon fibres in scanning electron microscope. The volume, and longitudinal and transverse moduli of a carbon fibre at three states of lithiation are determined and compared. The transverse modulus of the lithiated fibre is found to be more than double that of the pristine and delithiated fibres.

1. Introduction

Solid-state batteries have been extensively studied in last decade mainly for the safety concern [1,2]. Since the battery is solid, it also has the capability to carry mechanical load as a structural component [3]. The mechanical performance of a solid-state battery depends on the mechanical properties of its components, i.e. negative electrode, positive electrode, and solid-state electrolyte. Carbon fibres, especially the intermediate modulus (IM) polyacrylonitrile- (PAN-) based carbon fibres, have been proven as successful negative electrodes with similar energy density as most widely used graphite particle electrodes [4]. The elastic modulus of commercial graphite particles is normally around 10 GPa, while the PAN-carbon fibres have around 30 times higher modulus in its fibre direction. By employing carbon fibre electrodes, an optimized solid-state battery, known as structural battery composite, can have a modulus of 117 GPa in fibre direction with a low density of 2.56 g/cm^3 [5]. The specific modulus (the ratio of elastic modulus to density) of the structural battery composite (45.7 GPa/(kg/m^3)) is remarkably higher than that of steel (26.5 GPa/(kg/m^3)) and aluminium alloy (25.5 GPa/(kg/m^3)). In an electrical vehicle, structural battery composites have potential to reduce the total weight by 20–30% and thereby improve the driving range by up to 70% [6]. Recently, few groups have successfully fabricated structural battery composites using carbon fibres electrodes [7,8] and drew extensive attention.

Replacing the graphite electrode with a carbon fibre electrode in solid-state batteries is promising. Note that the carbon fibre electrode is embedded in a solid-state electrolyte. Changes in volume and elastic properties will introduce internal stresses, change the overall mechanical performance of the battery, and may cause damage to the battery. It is well-known that all electrode materials expand during lithium insertion. The volume change of an electrode varies between materials. Silicon is known to undergo extensive expansion upon lithiation. A volume change of 380% has been reported for silicon as lithium is inserted [9]. A more relevant comparison for carbon fibres is the expansion of graphite. For graphite a volume increase of 13.2% has been reported [10]. Recent theoretical studies, using multi-physics based finite element analysis, show that even a 5% radial expansion of the carbon fibre

* Corresponding author.
E-mail address: leif.asp@chalmers.se (L.E. Asp).

https://doi.org/10.1016/j.carbon.2021.09.037

electrode significantly affects the internal stress state and may cause cracks in the solid-state electrolyte matrix or debonding between the carbon fibre electrode and solid-state electrolyte [11,12]. To ensure mechanical integrity of a structural battery composite, it is vital to have reliable data on the change in fibre volume and elastic properties for the carbon fibre due to lithium insertion and desertion. However, the effect of lithium insertion on the elastic moduli of carbon fibres is still unknown.

The crystal structure of a carbon fibre is generally considered as turbostratic graphite. In a graphite crystal, graphene planes stack parallelly following a Bernal model (ABAB sequence) with an interlayer spacing of 3.35 Å. The graphene planes are bonded by van der Waals forces. Once the graphite is fully charged by lithium, LiC_6 crystal forms. The graphene planes shift and form an AA stacking sequence. Even though the interlayer spacing is increased to 3.7 Å, the interlayer bonding is strengthened by the formation of covalent bonds [13] or cation-pi interactions [14] between the carbon hexagons and lithium atoms. As a result, the elastic moduli of the graphite crystal change. Theoretical analysis of the graphite lattice showed both the out-of-plane (interlayer) elastic constant (C_{33}) and the shear elastic constant between graphene planes (C_{44}) to be increased by lithium-carbon bonding. The in-plane longitudinal elastic constant (C_{11}) is, however, decreased. The reduction in longitudinal modulus is inherent to the lattice expansion induced by lithiation, which increases the out-of-plane cross-section area and distance between carbon atoms. Experimental studies confirm these effects [15–17]. In carbon fibre, the graphene planes are also bonded by van der Waals bonds. However, the turbostratic graphitic structure implies misorientations between, and defects within, the graphene planes. This results in different physical properties compared to the perfect graphite crystal, such as a larger average interlayer spacing (3.49 Å for the IMS65 carbon fibre studied in this work [4]). In addition, carbon fibre crystals are usually small, down to a few nanometres and contain much more defects. This is proven by a strong D peak in the Raman spectrum [4]. Therefore, the stiffening effect of C_{33} and C_{44} and softening effect of C_{11} of a single crystal are expected to prevail, while their influence degrees can vary from that on graphite. Furthermore, the crystal orientation distribution is highly anisotropic in carbon fibres. The strong alignment of the graphene planes parallel to the fibre direction causes the longitudinal elastic modulus (i.e. along the fibre axis) to be significantly higher than in the radial (i.e. transverse) direction [4,18]. In the transverse plane (i.e. the fibre cross-section), the crystals are randomly oriented. The anisotropic crystal alignment will cause anisotropic effects on elastic properties from lithium insertion in the axial and transverse directions.

Until now, experimental measurements of the elastic moduli of lithiated and delithiated carbon fibres are still lacking. A main challenge is that lithiated carbon fibres quickly corrode in ambient environment. Protection must be ensured during specimen preparation, transportation, and experimental test. This is challenging for all air and moisture sensitive materials. Previous studies on lithiated graphite in the literature were performed using neutron diffraction on small single crystal or highly oriented pyrolytic graphite (HOPG) [15–17]. Direct mechanical measurements on lithiated components are very limited. Berla et al. conducted nanoindentation tests on lithiated silicon film [19]. The lithiated silicon was protected using paraffin oil and the test was performed in ambient environment. Thanks to the flat surface of the silicon anode, the nanoindentation test did not require precise control of the position of the sharp indenter tip. This is not the case for the lithiated carbon fibre. Firstly, the carbon fibre has a cylindrical shape. To use a sharp indenter tip, a flat carbon fibre surface is required. Conventional polishing methods cannot be used as water and oxygen react with the lithiated carbon fibre. Therefore, a flat punch, which does not require additional preparation of the carbon fibre is a better alternative. Flat indenters have been used to perform compression test on pristine carbon fibre in a few studies [20,21]. Secondly, to determine the modulus, the contact length between the indenter probe and specimen needs to be precisely measured. Due to the micro-scale of the carbon fibre diameter, this requires an advanced control and monitoring system.

In the present work we develop an experimental procedure and determine the elastic moduli of fully lithiated and delithiated IMS65 carbon fibres and compare these with the corresponding moduli of the pristine fibre. Both the longitudinal and the transverse moduli are determined. For this purpose, we measure the expansion of the carbon fibre cross-section area due to lithium insertion using scanning electron microscope (SEM). Homogenous expansion along the fibre is documented by high-resolution computed tomography (HR-CT). Longitudinal expansion is measured using an *in-situ* video microscopical method [22]. To protect the lithiated and delithiated carbon fibres during sample transportation, we cover the conditioned carbon fibre in a hydrophobic ionic liquid. The transverse modulus is measured by a compression test inside the SEM and found to be 2.07 times higher after lithium insertion.

2. Material and methods

2.1. Materials

The IMS65 fibre is studied for its high multifunctional properties and circular cross-section (i.e. cylindrical geometry) [4,18]. Even though the T800 carbon fibre has been more extensively used as the negative electrode in structural batteries [7,23], its “kidney-shaped” cross-section does not comply with the analysis method for radial compression of a cylinder. Unsized IMS65 carbon fibre is kindly provided by Toho Tenax, Germany. First lithiated and first delithiated IMS65 carbon fibres are prepared in half-cells with a lithium metal anode. Lithium hexafluorophosphate solution (1 M $LiPF_6$ in EC/DEC = 50:50 (v/v) purchased from Sigma-Aldrich) is used as electrolyte. Neware CT-4008-5V10mA-164 battery cycler is employed to cycle the half-cell. The cycling current is set as 0.1C rate based on the theoretical specific capacity of graphite (372 mA h/g). The slow charge rate is chosen to ensure full lithiation and delithiation states. The cycling window is set between 0.002 V and 1.5 V. After cycling, the half-cells are opened in an argon filled glove box (O_2 < 1 ppm, H_2O < 1 ppm) and the carbon fibres are quickly dried in vacuum. Stainless steel discs from Caspilor AB are polished using 1 μm diamond paste and used as substrate. The lithiated and delithiation IMS65 carbon fibres are fixed on the steel substrate with copper tape. Ionic liquid, 1-Butyl-1-methylpyrrolidinium bis(trifluoromethanesulfonyl)imide 99.9% purchased from SOLVIONIC is then used to cover the carbon fibres during sample transportation and subsequent compression tests.

2.2. Volume expansion characterisation

The transverse expansion is analysed from SEM images taken in JEOL JSM-7800F Prime. The diameters of IMS65 carbon fibres are measured using ImageJ from 269, 94 and 204 fibres for pristine, fully lithiated and delithiated specimens, respectively. The longitudinal expansion of a bundle IMS65 fibre is recorded using a USB3 camera mvBlueFox3-2064C with lens MV-OMC303-OE. The carbon fibre bundle is approximately 6 mm and glued on a copper current collector using PELCO® conductive silver paint. The specimen is cycled vs. a lithium metal anode using potentiostat Ivium OctoStat 30. The cycling curve is plotted in Supplementary Fig. S1. ImageJ is used to measure the pixel number along the fibre length. HR-CT is

employed to study the morphology of lithiated and deliathiated carbon. To protect the lithiated and delithiated carbon fibres from air, the carbon fibres are stored in polyimide tubes (ID:0.5 mm, length: 2 cm) purchased from Charles Supper company. Both ends of the tube are sealed using hot melt glue (Supplementary Fig. S2). X-ray nano-CT (XCT) characterization is performed to analyse the pristine carbon fibre, as well as the fully lithiated and delithiated fibres. Tomograms are acquired on a Zeiss Xradia 810 Ultra with a Cr X-ray source using the Zernike Phase contrast mode at a resolution of ~130 nm per cubic voxel. The data is reconstructed using Zeiss XM Reconstructor and then analysed with a custom Python script, which will be detailed in a future paper, to measure the fibres diameter. 3D renderings are created using ORS Dragonfly.

2.3. X-ray diffraction (XRD)

XRD is conducted in Mat:Nordic SAXS/WAXS/GISAXS. Cu Kα X-ray source is used. The 2θ scan is from 5 to 30°. The lithiated and delithiated IMS65 carbon fibres are ground to powder inside the glovebox. The powder is then poured into thin-walled quartz capillary tubes (ID: 1 mm, thickness: 0.1 mm) purchased from Charles Supper company. The end of the capillary is sealed using vacuum grease and holt melt glue.

2.4. Compression test

Transverse compression modulus for the IMS65 carbon fibre in its pristine, lithiated and delithiated states is measured by flat punch compression. The method has been proven able to measure the transverse modulus of pristine carbon fibres [20,21]. The lithiated and delithiated carbon fibres are protected from air and moisture by an ionic liquid cover to avoid undesired corrosion. Compression tests are performed using an *in-situ* nanoindenter from Alemnis AG with a 0.5 N load cell, mounted in a Zeiss LEO Ultra 55 SEM where high vacuum condition can be achieved. A tungsten carbide flat punch (ALM/FLT060/D100/WC/UHT (60° cone angle)) from Synton-MDP AG with a diameter of 107 μm is employed. As there is a risk that the substrate deforms plastically during the compression test, different maximum loads are tested (100 mN, 200 mN and 300 mN). A clear imprint of carbon fibre was observed after compression test with the 300 mN load. To avoid plastic deformation of the steel substrate, a maximum load of 150 mN is selected for all tests. Standard corrections for indenter frame compliance was applied.

The obtained unloading force-displacement curves are analysed to calculate the transverse modulus using relationships derived by Ward et al. [24–26]. The equations describe the diameter change of an anisotropic cylinder cross-section under transverse compression load as:

$$U = \frac{4F}{\pi}\left(\frac{1}{E_t} - \frac{\nu_{lt}^2}{E_l}\right)\left(0.19 + sinh^{-1}\frac{R}{b}\right) \quad (1)$$

$$b^2 = \frac{4FR}{\pi}\left(\frac{1}{E_t} - \frac{\nu_{lt}^2}{E_l}\right) \quad (2)$$

where.

U is the displacement of the indenter;

F is the transverse compression load per unit length along fibre axis;

E_t is the transverse modulus of the cylinder (*i.e.* the fibre);

E_l is the longitudinal modulus of the cylinder (*i.e.* the fibre);

ν_{lt} is the major Poisson's ratio;

R is the radius of the circular cross-section.

With assumption $\nu_{lt}^2/E_l \ll 1/E_t$, simplified Eqs. (3) and (4) are used.

$$U = \frac{4F}{\pi E_t}\left(0.19 + sinh^{-1}\frac{R}{b}\right) \quad (3)$$

$$b^2 = \frac{4FR}{\pi E_t} \quad (4)$$

3. Results and discussions

3.1. Fibre expansion due to lithium insertion

To determine fibre volume change from lithiation, we first measure the cross-section areas of IMS65 carbon fibres at three different states of lithiation (SOL). Cross-section areas for pristine fibres as well as for fibres after first lithiation and after a subsequent first delithiation are reported. These data are also used as input for the following compression test analysis and for calculating change in longitudinal modulus. The distributions of the cross-section areas (Fig. 1a) and expansion ratios (Table 1) are obtained from micrographs. An average cross-section area expansion of 13.7% is found after first lithiation. The XRD (Supplementary Fig. S3) also shows that the interlayer spacing (002) expands from 3.45 Å to 3.87 Å from lithiation. The measured interlayer spacing of pristine IMS65 carbon fibre is similar to the value 3.49 Å reported by Fredi et al. [4]. The interlayer spacing expansion ratio is consistent with the cross-section expansion ratio. This is larger than the 8.8% reported by Jacques et al. [27]. A cross-section area expansion of 13.7% can mainly be explained by the interlayer spacing increase due to lithium intercalation. The measured interlayer spacing expansion is larger than the interlayer spacing expansion of a graphite crystal (3.35 -> 3.70 Å), which is approximately 10% [10]. This is rational because the weak interlayer bonding and loose stacking structure in the carbon fibre are not sufficient to counteract the repulsive force between intercalated lithium atoms compared to a closely stacked graphite. This effect has been proven by the large interlayer spacing expansion of chemically reduced graphene oxide (rGO) in the work by Sun et al. [28]. The interspacing of rGO has been measured using XRD and found to increase by 21% from 3.42 to 4.15 Å due to lithium intercalation. After first delithiation, the fibre diameter is recovered. A slight negative expansion ratio is obtained corresponding to a 0.5% reduction in diameter. However, the average crystal interlayer spacing does not fully recover as the fibre is delithiated. XRD measurements reveals that the average interlayer spacing decreases to 3.72 Å after delithiation. This is larger than the initial interlayer spacing 3.45 Å. The larger interlayer spacing but unchanged volume of the delithiated carbon fibres compared with the pristine fibres suggest the expanded crystals are near inner voids (around 20% volume fraction, estimated from the density of IMS65 (1.78 g) and graphite (2.26 g)), where their expansion does not contribute to the fibre volume expansion.

Longitudinal fibre expansion is measured from a video of the carbon fibre electrode during electrochemical cycling (Fig. 1b). The video is recorded using an optical microscope and provided in Supplementary Movie 1, in which the longitudinal expansion of the fibres is visible. Here, longitudinal fibre expansions of 0.69% and 0% at first lithiation and after first delithiation, respectively, are measured (Table 1). Jacques et al. measured the longitudinal fibre expansion using a relaxation test to be 1.05% and 0.28% at lithiation and after delithiation, respectively [27]. Furthermore, the lithiated and delithiated carbon fibres are studied by HR-CT. 3D

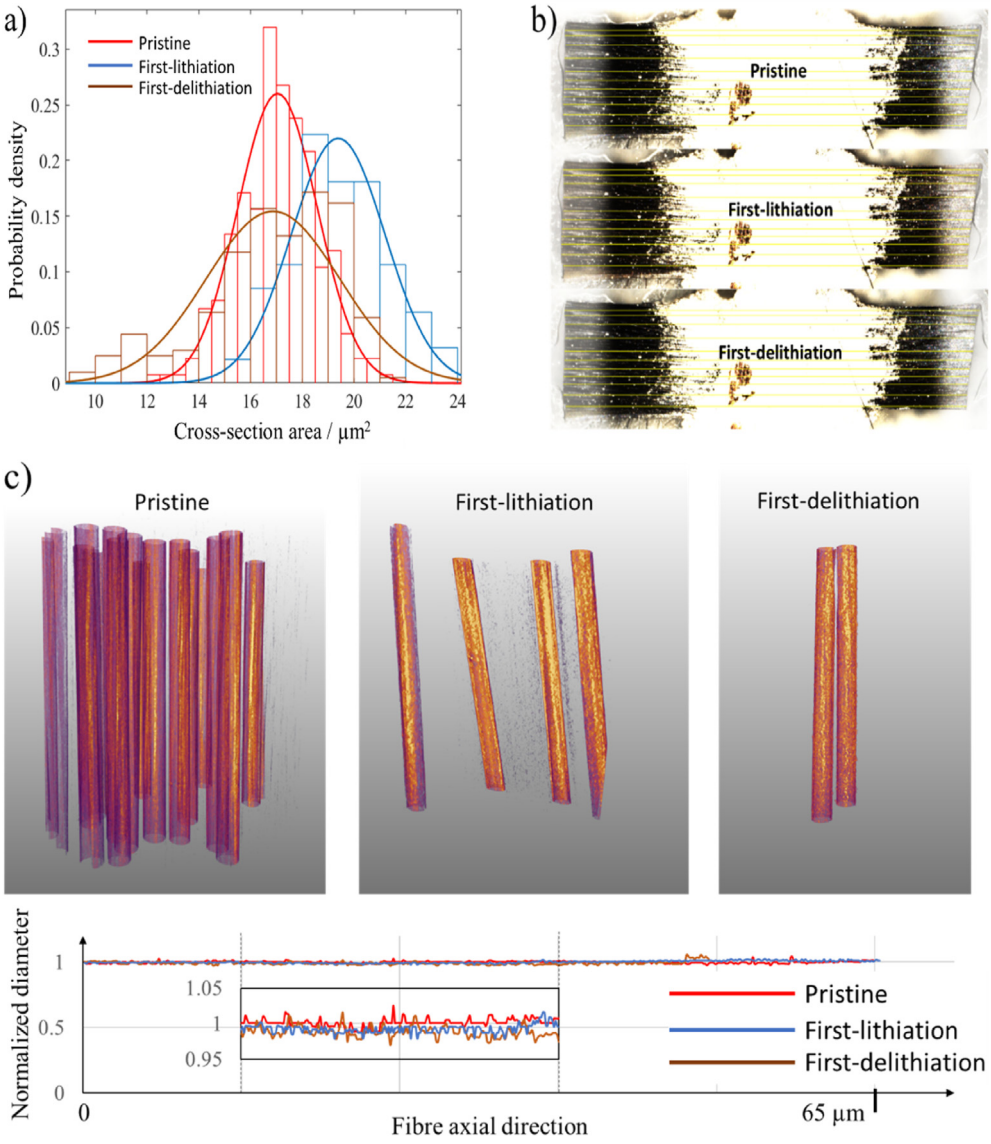

Fig. 1. Volume expansion of IMS65 carbon fibre at different SOL relative the pristine fibre. a) The probability density distribution of the cross-section areas of IMS65 fibres at different SOL. b) Images from video of the longitudinal expansion of the carbon fibre during electrochemical cycling (Pristine, end of first lithiation and after first delithiation). The brightness and contrast are modified in Affinity photo to make the ends of the carbon fibres more distinguishable. c) 3D reconstructions and normalized diameters along 65 μm long carbon fibre segments from HR-CT. Parts of the curves are zoomed-in to show the variation in diameter between ±5%. (A colour version of this figure can be viewed online.)

Table 1
Cross-section area of pristine IMS65 carbon fibres and their expansion in transverse and longitudinal directions after first lithiation and first delithiation.

SOL	Transverse direction			Longitudinal direction
	Mean cross area/μm²	Area expansion	Diameter expansion	Longitudinal expansion
Pristine IMS65	17.05 ± 1.53	–	–	–
Lithiated IMS65	19.39 ± 1.81	13.7%	6.6%	0.69%
Delithiated IMS65	16.87 ± 2.58	−1.1%	−0.5%	0%

reconstructions of carbon fibres at three different states are generated (Fig. 1c). The cylindrical geometry remains and the normalized diameters over a 65 μm long carbon fibre section are consistent for each SOL. This confirms that lithiation occurs homogenously along the fibres.

Supplementary video related to this article can be found at https://doi.org/10.1016/j.carbon.2021.09.037

3.2. Ionic liquid corrosion protection and its influence on compression test

During the installation process into the SEM the specimen is exposed to air for approximately 1 min. In addition, the specimen also risks exposure to air during the few minutes the SEM is evacuated. A battery electrolyte grade ionic liquid is therefore used to cover the carbon fibres. The ionic liquid is hydrophobic and as

such prevents absorption of moisture from air. The key features of the ionic liquid are good wetting ability, high electron conductivity and negligible vapour pressure. Good wetting ability ensures that the entire carbon fibre surface is covered. High electron conductivity and negligible vapour pressure are essential for use in the SEM. As a result, no charging effect, nor any evidence of evaporation of the ionic liquid is observed. The chamber pressure remained stable below 10^{-5} Pa during the experiment. Even though the carbon fibres are covered in the ionic liquid and cannot be directly observed in the SEM, their positions can still be recognized by the surface tension of the ionic liquid (Fig. 2a). A lithiated carbon fibre that has corroded shows dense and large dendrites up to 5 μm in dimension (Supplementary Fig. S4). Such large dendrites would be detectable even when covered in ionic liquid. In all experiments, no evidence of oxidation is observed. In addition, the compression curve for a corroded fibre specimen is expected to be discontinuous and unstable as the oxidation products are crushed. All compression curves (Supplementary Fig. S5) are smooth. Therefore, the oxidation of lithiated carbon fibre is avoided, or at least sufficiently low not to influence the compression test response.

Compression tests are performed in a nanoindenter (Fig. 2b) installed in the SEM. During the compression test, the ionic liquid completely covers the carbon fibres (Fig. 2a). The ionic liquid is not expected to influence the compression test result due to its great lubricity. To verify this, compression tests are performed on pristine carbon fibres with and without the ionic liquid cover (Fig. 2c). A small ionic liquid droplet and pristine carbon fibres are placed on a steel substrate. The droplet is kept at a distance from the pristine carbon fibres. Firstly, three clean pristine carbon fibres are compressed. The indentation probe is then moved and dipped into the ionic liquid droplet. As a result, a large amount of ionic liquid becomes attached to the indenter probe surface. With the wetted indentation probe, the three tested carbon fibres are compressed again at locations close to the previous compression tests of the bare fibres. The indentation curves are very similar for the individual fibres (Fig. 2d). The average extracted modulus are 6.7 ± 2.3

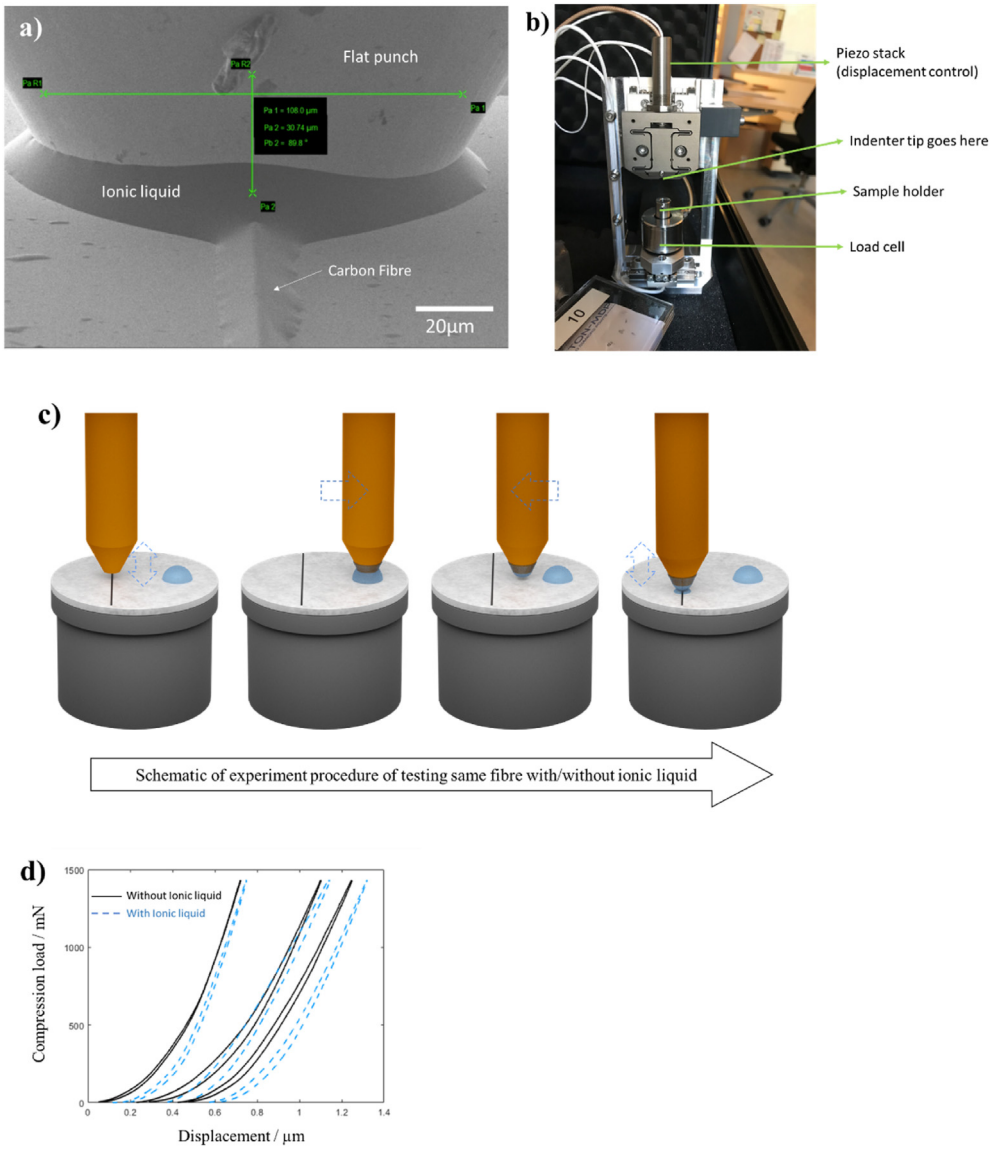

Fig. 2. Illustration of the setup for the compression test in the SEM. a) An *in-situ* SEM image during the compression test. b) Nanoindenter. c) Schematic illustration of the experimental steps in compression tests on same fibres with/without ionic liquid. d) Compression curves of pristine IMS65 carbon fibres with/without ionic liquid. (A colour version of this figure can be viewed online.)

and 6.7 ± 2.7 GPa when the fibres are tested with and without ionic liquid, respectively.

3.3. Effect of lithium insertion on the transverse modulus

The sample stage is pre-tilted at 20° with respect to the electron beam to allow visual access. To ensure the desired contact length between the carbon fibre and the flat punch, the flat punch is positioned with its centre on top of the carbon fibre. To achieve this, the carbon fibre needs to be aligned parallel to the electron beam. With the help of annotation tools, the carbon fibre can be moved to the centre line of the flat punch. However, the nanoindenter stage cannot be rotated inside the SEM. Therefore, the carbon fibres need to be pre-aligned manually outside the SEM. Note that this is a strict requirement since even a small misorientation (of a few degrees) will cause a large, conspicuous, deviation in fibre orientation due to the low angle of view (20°). Another requirement is that the distance between carbon fibres must be large enough to guarantee that only a single fibre is compressed in each test. Altogether, these requirements result in that only a limited number of fibres can be tested in one set up. Here, 8 to 12 fibres are tested at different SOL. Typical force-displacement curves for the different specimens are plotted in Fig. 3a. The steeper slope of the compression curve from the test of the lithiated carbon fibre implies an increased modulus from lithium insertion.

Combining with the measured diameter, the transverse compression modulus of IMS65 at different SOL is obtained (Fig. 3b and Table 2). The transverse compression modulus increases drastically from 7.4 ± 2.0 to 15.3 ± 2.6 GPa after the first lithiation and decreases to 7.6 ± 2.5 GPa after first delithiation. Consequently, the stiffening factor from lithiation is determined to be 2.07.

To understand the observed stiffening effect, the carbonaceous structure of the carbon fibre can be simplified as a mixture of graphite crystals with all graphene layers oriented in parallel to the fibre axis. Three main elastic stiffness components of the graphite crystal are considered, i.e. in-plane constant C_{11}, out-of-plane constant C_{33} and shear constant C_{44}. The graphite crystals become aligned along the fibre axis due to an external tensile load applied during manufacture. In contrast, as no force is acting in the radial direction the crystals are free to rotate around the fibre axis during manufacture. Indentation modulus across a polished IMS65 carbon fibre mid-surface was measured by nanoindentation tests in a recent study [18]. The indentation modulus was found constant along the diameter, *i.e.* normal to the fibre axis. Hence, the graphite crystals are considered to be randomly distributed in the transverse cross-section of the carbon fibre, *i.e.* unlike along the fibre axis, there is no preferred crystal orientation in the radial-hoop plane. Therefore, transverse compression modulus of the carbon fibre is

Table 2
Elastic moduli of IMS65 at different states of lithiation (pristine, lithiated and delithiated).

SOL	Elastic modulus/GPa (Stiffening factor)	
	In transverse direction	in longitudinal direction
Pristine fibre	7.4 (–)	290 (–)
Lithiated fibre	15.3 (2.07)	255 (0.88)
Delithiated fibre	7.6 (1.03)	293 (1.01)

related to a combination of C_{11}, C_{33} and C_{44} for the single crystals and their orientation. The three elastic constants, C_{11}, C_{33} and C_{44}, are affected differently by lithium intercalation. C_{33} and C_{44} increase due to the strengthened interlayer bonding by lithium and carbon hexagon interaction. In contrast, C_{11} decreases. There are at least two reasons for this. Firstly, the expanded carbon hexagons have larger carbon-carbon distance and therefore, a weaker carbon-carbon bond. Secondly, the number of graphene planes per unit volume is decreased due to the expanded lattice. Theoretical calculations presented in the literature suggest C_{33} to increase by a factor of 1.65–2.29 and C_{44} to increase more than 5 times, whereas C_{11} is predicted to decrease by a factor of 0.87 [13]. Considering the high value of C_{11} (1040 GPa) and much lower values of C_{33} and C_{44} (40 GPa and 3.0 GPa, respectively), and the fact that the measured transverse modulus of pristine IMS65 is as low as 7.4 GPa, the transverse elastic modulus of the fibre is found to be dominated by C_{33} and C_{44}. This is also true for the fibre's transverse stiffening factor. The obtained stiffening factor of 2.07, which lies between the computed increase in C_{33} and C_{44} confirms this.

Furthermore, since the graphite crystals are assumed to be randomly distributed in the plane normal to the fibre axis, the elastic response in the transverse direction should be similar to that of poly-crystal graphite. Qi et al. studied the effect from lithiation of a randomly distributed poly-crystal graphite using density functional theory (DFT) and found Young's modulus to increase by a factor of 3 [14]. The measured increase in transverse modulus of 2.07 for the carbon fibre is smaller than the predicted three-fold increase for poly-crystal graphite. First, DFT modelling assumes prefect crystals, whereas real poly-crystalline graphite can have a significantly different deformation mechanism [29]. Second, the IMS65 carbon fibre consists of turbostratic graphite. High defect content of IMS65 carbon fibre is proven from the Raman spectrum captured by Fredi et al. [4]. Although the lithiation effect on the stiffening factor in the presence of a large number of defects and misorientations in the IMS65 fibre's carbonaceous microstructure is unknown, it is rational to be lower than for graphite. Fredi et al. [4] found the Li-ion insertion mechanism in IMS65 fibres to be close to that of partly disordered carbons. A part of the lithium atoms is

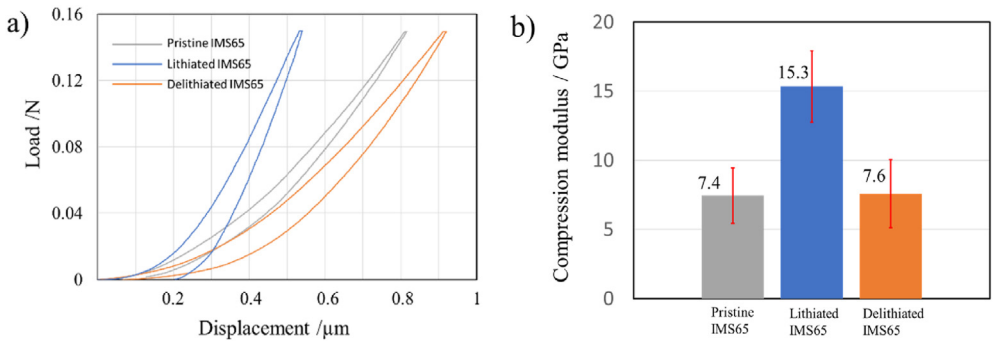

Fig. 3. Transverse modulus of IMS65 at different SOL. a) Typical force-displacement curves from the compression tests. b) The transverse compression modulus of IMS65 at different SOL (pristine, first-lithiation and first-delithiation). (A colour version of this figure can be viewed online.)

stored at defects. Additionally, the specific capacity of the IMS65 fibre is lower than the theoretical specific capacity of graphite (372 mA h g^{-1}). The 1st cycle capacity, and hence the lithium content, of the IMS65 fibre (Supplementary Fig. S6) is approximately 90% of the theoretical specific capacity of graphite. Furthermore, part of the lithium atoms forms a solid electrolyte interphase (SEI) layer. In total, less lithium is inserted into the graphitic interlayer structure inside the fibre. Lithium atom intercalation in the graphitic structure is the source for the stiffening effect. Therefore, the lower amount of intercalated lithium in the IMS65 fibre results in a lower stiffening factor compared to that for graphite.

The measured transverse compression modulus of pristine IMS65 fibres is similar to that found in other studies using similar compression test methods [20,21]. However, the transverse modulus is remarkedly lower than that measured by sharp indentation tests. In a previous study, using indentation tests in an atomic force microscope (AFM), the transverse modulus of the IMS65 fibre was found to be 21.8 GPa [18]. The previously developed method could not be applied here due to constraints related to transfer between instruments and required machining in the FIB/SEM. There are numerous reasons for the difference in measured transverse modulus between the test methods. The most obvious reason is the difference in indenter probe geometry. A flat punch is used in the current work, whereas a sharp indenter probe with spherical tip was used in the previous study. Sharp indentation has also been used in a few studies in the open literatures [30–32]. All of them obtain transverse moduli of different carbon fibres higher than 10 GPa, most of them are higher than 20 GPa. In contrast, compression tests in general give a transverse modulus lower than 10 GPa [20,21]. As an example, for the T300 carbon fibre transverse compression tests determined the transverse modulus to be between 6.05 [20] and 7.79 GPa [21], whereas an indentation test measured its transverse modulus to be 27.6 GPa [30]. The lower modulus from compression tests may result from the porous structure of carbon fibres. While the compression test generates deformation of the entire fibre, the indentation tests only cause local deformation. All sharp indentation experiments on carbon fibres to date are performed over a distance less than 200 nm. In another aspect, the poly-crystalline graphite shows a lower effective modulus due to a different deformation mechanism [29]. The larger number of crystals involved during compression test therefore exhibits a lower effective modulus.

It is also noted that the transverse modulus of the delithiated carbon fibre is recovered, like the fibre volume, even though around 25% of the lithium atoms are trapped in the carbon fibre (Supplementary Fig. S6). The amount of trapped lithium atoms is too high to be contained only in the SEI layers on the carbon fibre surface, considering the specific surface of the carbon fibre is much lower than for normal anode graphite particles. According to Ng et al. [33], a graphite anode with three times the specific surface area of the IMS65 carbon fibre has a first cycle loss of less than 15%. Consequently, the 25% first cycle loss for IMS65 suggests that a large amount of lithium is trapped inside of carbon fibre. However, since the trapped lithium atoms are found not to stiffen the delithiated carbon fibres, the lithium atoms are indicated to be trapped at defects, such as grain boundaries and voids.

3.4. Effect of lithium insertion on the longitudinal modulus

Longitudinal modulus of the IMS65 carbon fibre is not measured directly in this work. It is calculated from the change in cross-section area. This can be done as the stiffness of the IMS65 fibre has been demonstrated unaffected by lithium concentration, *i.e.* at different SOL [34]. Jacques et al. performed tensile tests on IMS65 carbon fibre yarns and found no effect on stiffness during electrochemical cycling. Consequently, the change in longitudinal elastic modulus is the reciprocal to the change in cross-section area as

$$\Delta E = \frac{S}{\Delta A}, \tag{5}$$

where S is the stiffness, ΔA is the change in cross-section area and ΔE is the change in Young's modulus. The longitudinal modulus of pristine IMS65 carbon fibre is given in the data sheet from the carbon fibre manufacturer. The longitudinal modulus at different SOL are calculated and listed in Table 2. The softening factor from first lithiation in the axial direction is 0.88. It is very similar to the softening factor of C_{11} (0.87) for graphite.

4. Conclusions

An experimental method to study the elastic properties of lithiated micro-scale components is demonstrated. From volume change measurements and compression tests we have confirmed a dramatic effect of lithium insertion on the transverse modulus of a carbon fibre used as negative electrode in lithium-ion batteries, such as structural battery composites. The transverse modulus of the IMS65 carbon fibre is found to more than double when fully lithiated. In contrast, its longitudinal modulus is slightly decreased. The change in elastic moduli is explained by lithium intercalation in the turbostratic graphitic crystal structures of the carbon fibre, as well as from the caused increase in fibre volume. The volume and moduli are practically recovered as the fibre is delithiated. Equipped with this information, electro-chemo-mechanical analyses can be performed to explore arbitrary solid-state battery designs, e.g. structural battery composites.

CRediT authorship contribution statement

Shanghong Duan: Formal analysis, Data curation, conceived and designed the experiment, prepared the specimens for experiments, measured the cross-section expansion and XRD, analysed the compression data, Writing – original draft, wrote the manuscript, Writing – review & editing, All authors reviewed and commented the manuscript. **Anand H.S. Iyer:** performed the compression test, Writing – review & editing, All authors reviewed and commented the manuscript. **David Carlstedt:** conceived and designed the experiment, Writing – review & editing, All authors reviewed and commented the manuscript. **Florian Rittweger:** performed the longitudinal expansion experiment, Writing – review & editing, All authors reviewed and commented the manuscript. **Andrew Sharits:** performed HRCT experiment, Writing – review & editing, All authors reviewed and commented the manuscript. **Calvin Maddox:** performed HRCT experiment, Writing – review & editing, All authors reviewed and commented the manuscript. **Karl-Ragmar Riemschneider:** Writing – review & editing, All authors reviewed and commented the manuscript, were responsible for the, Funding acquisition. **David Mollenhauer:** conceived and designed the experiment, Writing – review & editing, All authors reviewed and commented the manuscript, were responsible for the, Funding acquisition. **Magnus Colliander:** conceived and designed the experiment, Writing – review & editing, All authors reviewed and commented the manuscript, were responsible for the, Funding acquisition. **Fang Liu:** conceived and designed the experiment, Writing – review & editing, All authors reviewed and commented the manuscript. **Leif E. Asp:** conceived and designed the experiment, Writing – original draft, wrote the manuscript, Writing – review & editing, All authors reviewed and commented the manuscript, were responsible for the, Funding

acquisition.

Declaration of competing interest

The authors declare that they have no known competing financial interests or personal relationships that could have appeared to influence the work reported in this paper.

Acknowledgements

This project has been funded by the European Union, Clean Sky Joint Undertaking 2, Horizon 2020 [Grant Agreement Number 738085]; USAF [contract FA9550-17-1-0338]; the German Ministry for Economic Affairs and Energy (BMWi) within the project 'IMBAT' [grant ZF4019009RE7]; and the Swedish National Space Agency [contract 2020-00256], which are gratefully acknowledged. This work was performed in part at the Chalmers Material Analysis Laboratory, CMAL.

Appendix A. Supplementary data

Supplementary data to this article can be found online at https://doi.org/10.1016/j.carbon.2021.09.037.

References

[1] Q. Zhao, S. Stalin, C. Zhao, L.A. Archer, Designing solid-state electrolytes for safe, energy-dense batteries, Nat. Rev. Mater. 5 (2020) 229–252.
[2] S. Kalnaus, L.E. Asp, J. Li, G.M. Veith, J. Nanda, C. Daniel, X. Chen, A. Westover, N.J. Dudney, Multifunctional approaches for safe structural batteries, J. Energy Storage 40 (2021) 102747.
[3] L.E. Asp, E.S. Greenhalgh, Structural power composites, Compos. Sci. Technol. 101 (2014) 41–61.
[4] G. Fredi, et al., Graphitic microstructure and performance of carbon fibre Li-ion battery electrodes, Multifunct. Mater. 1 (2018), 015003.
[5] D. Carlstedt, E. Marklund, L.E. Asp, Effects of state of charge on elastic properties of 3D structural battery composites, Compos. Sci. Technol. 169 (2019) 26–33.
[6] D. Carlstedt, L.E. Asp, Performance analysis framework for structural battery composites in electric vehicles, Compos. B Eng. 186 (2020) 107822.
[7] L.E. Asp, et al., A structural battery and its multifunctional performance, Adv. Energy Sustain. Res. 2 (2021) 202000093.
[8] K. Moyer, C. Meng, B. Marshall, O. Assal, J. Eaves, D. Perez, R. Karkkainen, L. Roberson, C.L. Pint, Carbon fiber reinforced structural lithium-ion battery composite: multifunctional power integration for CubeSats, Energy Stor. Mater. 24 (2020) 676–681.
[9] L. Christensen, M.N. Obrovac, Structural changes in silicon anodes during lithium insertion/Extraction, Electrochem. Solid State Lett. 7 (2004) A93–A96.
[10] S. Schweidler, et al., Volume changes of graphite anodes revisited: a combined operando X-ray diffraction and in situ pressure analysis study, J. Phys. Chem. C 122 (2018) 8829–8835.
[11] J. Xu, J. Varna, Matrix and interface microcracking in carbon fibre/polymer structural micro-battery, J. Compos. Mater. 53 (2019) 3615–3628.
[12] D. Carlstedt, K. Runesson, F. Larsson, J. Xu, L.E. Asp, Electro-chemo-mechanically coupled computational modelling of structural batteries, Multifunct. Mater. 3 (2020), 045002.
[13] K.R. Kganyago, P.E. Ngoepe, Structural and electronic properties of lithium intercalated graphite LiC6, Phys. Rev. B 68 (2003) 205111.
[14] Y. Qi, et al., Threefold increase in the Young's modulus of graphite negative electrode during lithium intercalation, J. Electrochem. Soc. 157 (2010) A558–A566.
[15] Q. Wang, et al., Thermal behavior of lithiated graphite with electrolyte in lithium-ion batteries, J. Electrochem. Soc. 153 (2006) A329–A333.
[16] P. Zhou, J.E. Fischer, Interlayer interactions in LiC 6: compressibility and thermal expansion, Phys. Rev. B 53 (1996) 12643.
[17] W.A. Kamitakahara, Dynamics of li-carbon and carbon solids, J. Phys. Chem. Solid. 57 (1996) 671–676.
[18] S. Duan, F. Liu, T. Pettersson, C. Creighton, L.E. Asp, Determination of transverse and shear moduli of single carbon fibres, Carbon 158 (2020) 772–782.
[19] L.A. Berla, S.W. Lee, Y. Cui, W.D. Nix, Mechanical behavior of electrochemically lithiated silicon, J. Power Sources 273 (2015) 41–51.
[20] S. Kawabata, Measurement of the transverse mechanical properties of high-performance fibres, J. Text. Inst. 81 (1990) 432–447.
[21] K. Naito, Y. Tanaka, J. Yang, Transverse compressive properties of polyacrylonitrile (PAN)-based and pitch-based single carbon fibers, Carbon 118 (2017) 168–183.
[22] F. Rittweger, Ch Modrzynski, V. Roscher, D.L. Danilov, P.H.L. Notten, K.-R. Riemschneider, Investigation of charge carrier dynamics in positive lithium-ion battery electrodes via optical in situ observation, J. Power Sources 482 (2021) 228943.
[23] W. Johannisson, et al., Multifunctional performance of a carbon fiber UD lamina electrode for structural batteries, Compos. Sci. Technol. 168 (2018) 81–87.
[24] D.W. Hadley, I.M. Ward, J. Ward, The transverse compression of anisotropic fibre monofilaments, Proc. Roy. Soc. Lond. A 285 (1965) 275–286.
[25] P.R. Pinnock, I.M. Ward, J.M. Wolfe, The compression of anisotropic fibre monofilaments. II, Proc. Roy. Soc. Lond. A 291 (1966) 267–278.
[26] S.A. Jawad, I.M. Ward, The transverse compression of oriented nylon and polyethylene extrudates, J. Mater. Sci. 13 (1978) 1381–1387.
[27] E. Jacques, M.H. Kjell, D. Zenkert, G. Lindbergh, M. Behm, Expansion of carbon fibres induced by lithium intercalation for structural electrode applications, Carbon 59 (2013) 246–254.
[28] Y. Sun, et al., Comparison of reduction products from graphite oxide and graphene oxide for anode applications in lithium-ion batteries and sodium-ion batteries, Nanoscale 9 (2017) 2585–2595.
[29] A. Mukhopadhyay, et al., Thin film graphite electrodes with low stress generation during Li-intercalation, Carbon 49 (2011) 2742–2749, https://doi.org/10.1016/j.carbon.2011.02.067.
[30] T. Csanádi, D. Németh, C. Zhang, J. Dusza, Nanoindentation derived elastic constants of carbon fibres and their nanostructural based predictions, Carbon 119 (2017) 314–325.
[31] K. Shirasu, K. Goto, K. Naito, Microstructure-elastic property relationships in carbon fibers: a nanoindentation study, Compos. B Eng. 200 (2020) 108342.
[32] T.S. Guruprasad, et al., On the determination of the elastic constants of carbon fibres by nanoindentation tests, Carbon 173 (2021) 572–586.
[33] S.H. Ng, et al., Correlations between surface properties of graphite and the first cycle specific charge loss in lithium-ion batteries, Carbon 47 (2009) 705–712.
[34] E. Jacques, et al., Impact of electrochemical cycling on the tensile properties of carbon fibres for structural lithium-ion composite batteries, Compos. Sci. Technol. 72 (2012) 792–798.